Sensors & Transducers, Vol. 245, Issue 6, October 2020, pp. 57-64

www.sensorsportal.com

Sensors & Transducers

Published by IFSA Publishing, S. L., 2020
http://www.sensorsportal.com

Indoors Geolocation Based on Visible Light Communication

[1, 2, *] Paula Louro, [1, 2, 3] Manuela Vieira and [1, 2] Manuel Augusto Vieira

[1] Electronics Telecommunication and Computer Dept. ISEL-IPL,
R. Conselheiro Emídio Navarro, 1959-007 Lisboa, Portugal
[2] CTS-UNINOVA, Quinta da Torre, Monte da Caparica, 2829-516, Caparica, Portugal
[3] DEE-FCT-UNL, Quinta da Torre, Monte da Caparica, 2829-516, Caparica, Portugal
Tel.: + 351218317000,
[*] E-mail: plouro@deetc.isel.ipl.pt

Received: 10 August 2020 /Accepted: 14 September 2020 /Published: 30 October 2020

Abstract: This paper presents the use of a selective device based on a-SiC:H/a-Si:H for the photodetection of visible signals emitted by red, green and blue emitters in a Visible Light Communication (VLC) system. The VLC system employs RGB white LEDs to provide both illumination and information transmission. The acquisition and processing of the measured photocurrent allows the identification of the induced optical excitation, which encodes the spatial position. The system is designed so that the detector's s spatial location can be obtained based on the identification of the received optical signals. The methodology used for the photocurrent signal processing involves Fourier transform analysis for frequency identification and the use of a photodetector with spectral selective properties of wavelength identification. A full characterization of the photodetector is presented together with the physical operation that plays the key role in the detection of the output photocurrent.

Keywords: Visible Light Communication, Indoor navigation, Bidirectional Communication, Optical sensors, Transmitter/receiver, White LEDs, Amorphous SiC.

1. Introduction

Visible Light Communication (VLC) technology constitutes a data communication tool based on the use of visible light that is used for illumination and data transmission [1-2]. These optical links use LEDs to encode and transmit the signals, and electronic devices generally containing photodiodes to detect the incoming signals from the light sources [3]. It is a free-space, line of sight communication technology [4]. Main advantages when compared to radio technology are free licensed spectrum, immunity from electromagnetic interference and, less power and weight/volume requirements [5].

Several applications are currently being developed, spanning from low data rate applications, such as indoor positioning and navigation to more demanding bandwidth applications [6-7]. Indoor navigation based on VLC [8] are useful solutions for Indoor Positioning Systems, as Global Positioning Systems (GPS) signals are attenuated by wall buildings. Thus, wireless solutions are commonly used. The main advantage of VLC over other wireless technologies ids related to the presence of visible light beacons in the buildings infra-structure, which provide a higher number of access points when compared to Wi-Fi.

In this paper, we propose the use of a multilayered a-SiC:H device [9] to perform the photodetection task at the reception end of a VLC system designed for navigation purposes [10-11]. The emission optical system is based on RGB white LEDs with the internal red, green and blue emitting chips being modulated at specific frequencies through coding bit sequences

normally based on On-Off keying [12-13]. The photodetector works as an active optical filter operating in the visible part of the electromagnetic spectrum [14]. Its sensitivity can be adjusted through external optical bias supplied by a steady state optical source. This is the key for light wavelength discrimination [15-16].

The paper is structured as follows. In Section II, the design of the VLC system is described. Section III contains results and respective discussion. Section IV presents main conclusion and a few guidelines for future work.

2. Architecture of the VLC System

The proposed optical system [17] can be described using the block diagram shown in Fig. 1. It contains two main sub-systems, one related to the input optical signal and a second one to the output electrical signal.

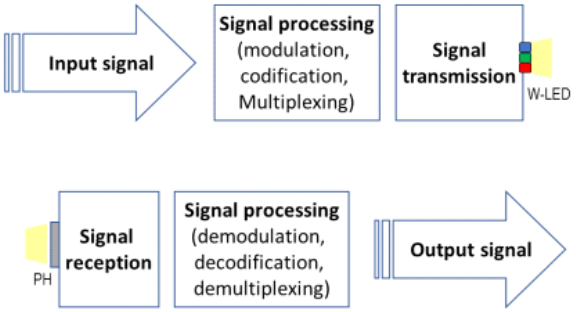

Fig. 1. Block diagram of the visible light communication system.

2.1. Transmitter

The input optical signal sub-system includes four white LEDs in which the internal emitting red, green and blue chips are modulated with specific frequencies and bit sequences inducing different optical excitations in the view angle of each LED. The output signal sub-system includes a large area a-Si based photodetector operating in the visible spectrum with a selective spectral photo response depending on external conditions (electrical and/or optical bias). The photocurrent signal produced by the photodetector is dependent on the input optical system. Signal processing at this stage includes demodulation of the electrical signal for demultiplex the different components assigned to each input wavelength, frequency analysis, and bit sequences decoding. The optical sources are commercial white LEDs with red, green and blue emitters (w-RGB LEDs). Specifications of the w-RGB LEDs are displayed in Table 1.

The commercial tri-chromatic white LEDs are designed for general lighting, providing a wide divergence angle around 120ºC, which fits simultaneously the requirements for illumination and communication services as it provides a wide signal distribution. The luminous intensity of each emitter can be independently adjusted; however, it must be regulated to ensure a stable, white perception by the human eye.

Table 1. RGB LEDs Specifications.

	Blue	Green	Red
Central wavelength (nm)	464	535	630
Linewidth (nm)	22	48	13
Optical intensity (mcd)	180 - 505	560 - 1400	355 - 900
Far field pattern, 2θ (º)	180 - 505	560 - 1400	355 - 900

The proposed optical sub-system for the VLC system (Fig. 2) includes several navigation cells with four white LEDs modulated with different bit sequences. Green emitters transmit the identification code of the navigation cell. Red emitters are used to transmit the western cardinal directions and the blue chips the eastern directions. North and South directions are ascribed to the modulation frequency. Frequency of the North positions is half of the one used for the emitters assigned to the South directions.

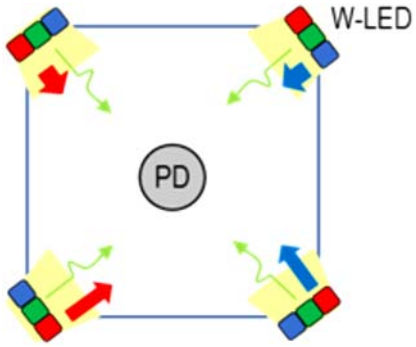

Fig. 2. Configuration of the luminaires used for illumination and communication.

The optical signal generated by the four LEDs and detected by the photodetector is spatially assigned its position, which provides a direct correlation of the measured induced photocurrent to the detector position [18].

2.2. Coder

The coder converts data into a modulated optical message to be transmitted by each white-LED. The driving current of each emitter is controlled independently suppling the respective coding sequence and frequency. An on-off keying modulation scheme was used with a 32-bit codification (1: light on

and 0: light off). The 32 bit word used to modulate the emitters of the white LEDs was divided into three main blocks related to synchronization, position information and message.

In every word 8 bits are allocated for synchronization of the transmitted frames: four bits at the beginning of the bit sequence with two idle bits and two start bits and four bits at the end of the sequence with two stop and two idle bits. Following the idle and start bits, 8 bits are reserved for positioning information. The green emitters carry the identification of the navigation unit cell, i.e., of the luminaire, and the modulated blue and red emitters the location inside the cell (north, south, west and east). The remaining 16 bits of the blue/red emitters are allocated for random message transmission, while the green emitters are set to the off state (this simplifies the decoding process and keeps free additional transmission channels for further enhancement of bandwidth if necessary). The 32 bits code word for the green emitters is: ´1100 0XX0 0YY0 00000000 00000000 0011´. For the top red and blue emitters it is: ´1100 0000 111 _ _ _ _ _ _ _ _ _ _ _ _ _ _ _ _ 0011´ and for the bottom red and blue emitters: ´1100 0011 0011 _ _ _ _ _ _ _ _ _ _ _ _ _ _ _ _ 0011´.

The luminaires are sequentially numbered as if in a matrix. A code word 8 bits long is reserved to address the line and column position of the cell, using the format 0XX0 for the line and 0YY0 for the column.

In Fig. 3 it is displayed the representation of adjacent navigation cells defined by the ceiling luminaire. Numbers 01, 02, … of the figure relate to the identification of each navigation unit cell. The zoom out corresponds to the configuration of the white LEDs inside the luminaire (Fig. 1).

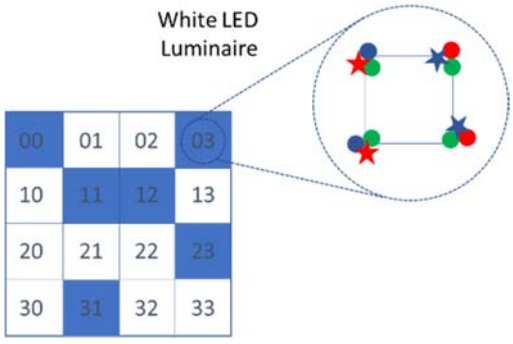

Fig. 3. Matrix of adjacent luminaires and zoom-out of a white LED luminaire. Modulated red/blue emitters are represented by a star.

2.3. Device Configuration and Characterization

Fig. 4 shows the semiconductor configuration used as integrated photodetector and tunable filter device. It is a monolithic heterojunction composed by two pin structures based on a-Si:H and a-SiC:H built on a glass substrate covered by two transparent electrical contacts. The device was fabricated by PECVD at 13.56 MHz radio frequency.

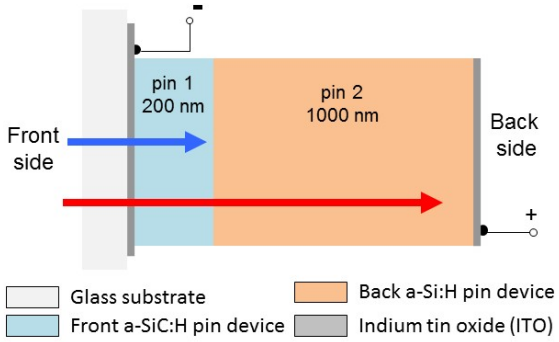

Fig. 4. Device configuration.

The intrinsic absorber materials of the pin devices were designed to confer the ability to detect separately short and long visible wavelengths. This assumption led to the engineering design of both intrinsic layers in what concerns thickness and material optical absorption coefficients, resulting in the choice of a narrow (200 nm) high bandgap (2.1 eV, a:SiC:H) material for the front layer and a thicker (1000 nm) lower (1.8 eV, a-Si:H) bandgap semiconductor for the back structure. Thus, the front p-i-n structure (pin1) exhibits high absorption to the blue light (shorter wavelengths) and high transparency to the red wavelength while the back structure (pin2) high absorption of the red wavelength. In Fig. 5, it is displayed the photodetector transient photocurrent under light produced by the blue, green and red emitters. In this experiment, each emitter was electrically modulated by a rectangular impulse generating a rectangular optical impulse on the device front side. The photocurrent was measured using steady state background lights from the front and back sides and without optical bias.

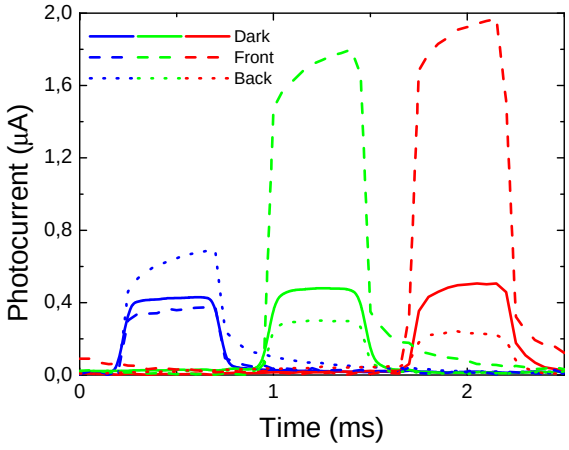

Fig. 5. Photodetector photocurrent measured without optical bias and under front and back optical bias under blue, green and red light of the white LEDs.

Results show that under back violet background illumination the gain is high at short wavelengths (blue light) and decreases for longer wavelengths (green and red). The device behaves as a short-pass filter. Under front violet background light, the device works as a long-pass filter for wavelengths above 500 nm, blocking the shorter wavelengths. The shift of the irradiation device side (front/back) allows tuning the short- and long- spectral regions, while the medium region (475 nm - 530 nm) can only be tuned by using both active filters. Under front illumination the red part of the spectrum is enhanced while under back illumination the main enhancement occurs for the blue signal. The quantification of the signal amplification under front and back bias is determined by the optical gain (α_F and α_B for the front and back gains, respectively), defined at each wavelength (λ) as the ratio between the signal magnitudes measured with and without optical bias.

For the red, green and blue light the front optical gain under violet background light is, respectively, 5, 3.5 and 1.3, while for the back optical gains, the values are 0.6, 0.6 and 1.7.

2.4. Decoding Algorithm

The decoding procedure for correct assignment of the photocurrent signal to the correspondent optical excitation involves several tasks summarized in Fig. 6.

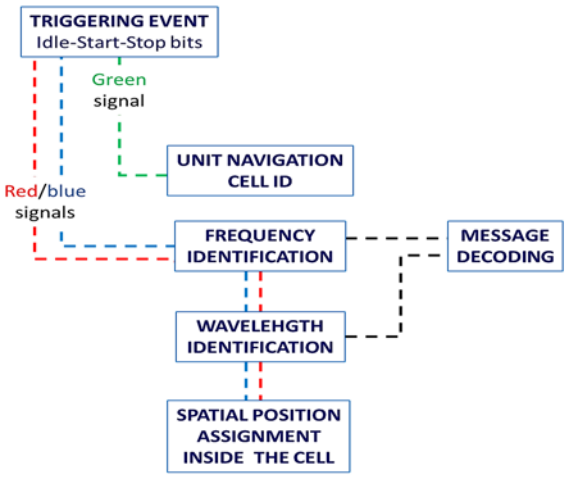

Fig. 6. Decoding tasks.

The start-idle bits allow easy synchronization and identification of each transmitted frame by the high peaks of the front photocurrent (represented by the magenta line), as in the idle bits all emitters are set to ON and this combination results in photocurrent amplification when the device is soaked by steady state illumination from the front side. By opposition, the same signal under back background light is decreased. After this identification, it is necessary to remove the contribution of the green signals from the photocurrent signal.

The next step is the identification of the transmitted frequencies, which requires the computation of the modulus of the complex Fourier coefficients over the 8 bits data sent next to the idle and start bits. When the calculated coefficient is above a certain threshold the signal is present at the respective frequency. In this step the front photocurrent is used to identify the red light and the back photocurrent for the blue light. This procedure enables the identification of the position within the navigation cell, which mixed with the cell identification by the green channel enables the absolute position recognition. The transmitted message is decoded using the adjacent 16 bits of the slow and fast emitters. If all the blue and red emitters transmit the same message as happens in data of Fig. 5, the decoding is based on the device filtering properties when optically soaked with front and back steady state light. The algorithm assumes that in the front photocurrent the highest levels correspond to the presence of the red light, while the lowest ones to its absence, which allows the immediate recognition of the ON-OFF states for the red channel. Regarding the back photocurrent signal, the same reason can be used. Here the highest levels are assigned to the presence of the blue input signal and the lowest levels to its nonexistence, which allows the immediate decoding of the blue channel. Thus, both red and blue channels can be immediately tuned by using adequate biasing light for the background and the bit sequence of the message can be decoded. However, for enlarging the channel capacity it is desirable that red and blue emitters transmit independent, different messages.

3. Results

Fig. 7 displays the output photocurrent signals, measured with and without front and back optical violet bias, in a specific position corresponding to the optical excitation from the red and blue emitters at the same frequency and a green signal for identification purposes.

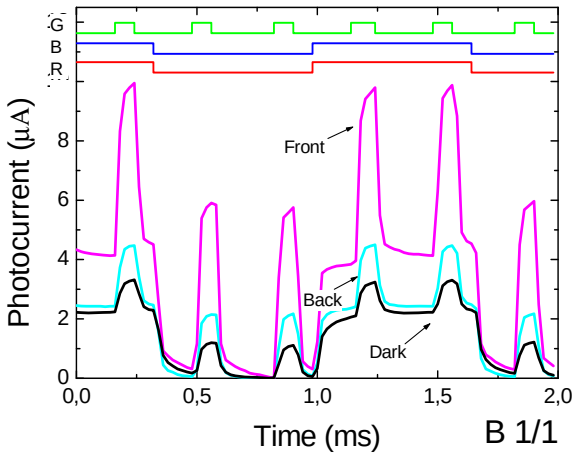

Fig. 7. Photocurrent signal measured without and under front and back optical bias.

The condition assigned when all optical signals are off corresponds to the reference level. The single optical signals are displayed at the top of the figure to help the reader with the different on-off optical states.

In this specific spatial position, the device receives three different optical excitations from the red, blue and green emitters. Under front background light the photocurrent is enhanced compared to the signal measured without background light, as the presence of the red and green light signals induce large amplification. Under back background light, the photocurrent signal is like the one measured without background, as there is a balance between the amplification factor due to the blue signal and the attenuation (α_F <1) from both red and green lights.

Based on the measured photocurrent, we have implemented a computer algorithm to automatically decode the individual photocurrents assigned to the different input optical signals. We started by extracting the green signal from the photocurrents, which was achieved by sampling the photocurrent signal at the specific time slots where the green signal logic state is unknown and subtracting it to the contiguous time slots where green is known to be absent (Fig. 8).

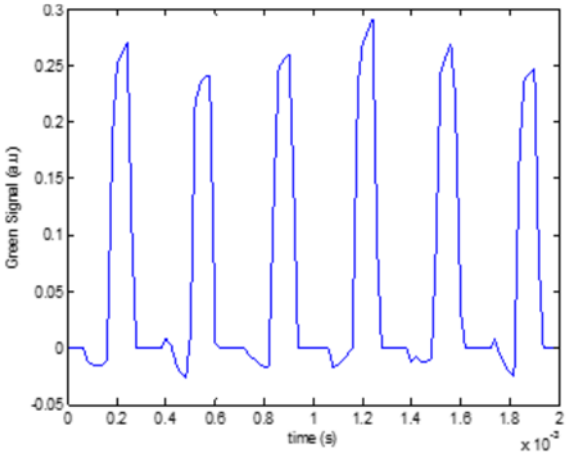

Fig. 8. Extraction of the signal encoded in the green channel.

The second step of the proposed algorithm is to filter out the green signal by simply subtracting the extracted green signal from the photocurrents. The third step takes advantage of the color filtering properties of the sensor. We use front optical biasing to detect green and red wavelengths and back biasing for the blue light. The modulus of the complex Fourier coefficients is computed. Decision about the presence of the frequency in the signal is taken if the evaluated coefficient is higher than a specific threshold. A dedicated algorithm built with MatLab was developed to automatically decode the location position of the detector.

In Fig. 9, it is displayed the Fourier coefficients obtained from the photocurrent signal measured under front and back optical bias. As the output signals can be described by square waves, they contain only components of odd-integer harmonic frequencies. The Fourier analysis shows that the detected frequency is around 750 Hz, which indicates that it is due to emitters located at the top of the unit cell (excited with R and B signals at this frequency). The observed low intensity signal at 1500 Hz is the resultant second harmonic caused by a non-perfect square wave. Results show that there is balance between both Fourier coefficients, which informs about the simultaneous presence of red and blue signals. This is clearly noticeable by the high peaks of the front photocurrent (represented in the graphs by the magenta line), as in the idle bits all emitters are set to ON and this combination results in photocurrent amplification when the device is soaked by steady state illumination from the front side. In contrast, the same signal under back background light is decreased.

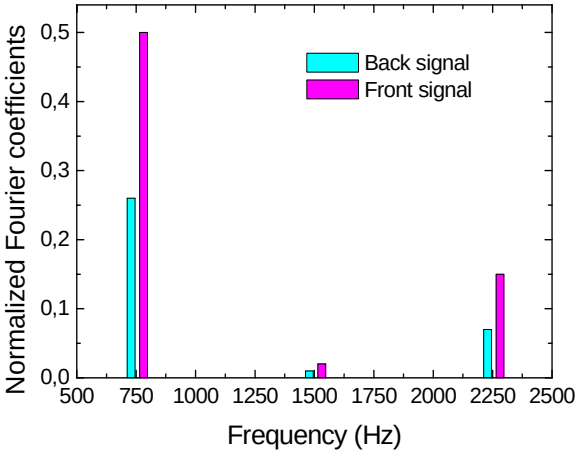

Fig. 9. Fourier coefficients obtained from the photocurrent signal measured under front and back optical bias.

4. Discussion

This decoding strategy is robust enough for the identification of the transmitted frequencies by top and bottom emitters, as the design of this code block is known. However, it does not happen with the identification of the transmitted message by the two red and two blue emitters. In this block there is a random distribution of the on-off bits in each channel. Thus, a new approach is needed for the transmission of different messages using the same wavelength, to demultiplex the photocurrent signal.

In Fig. 10 it is displayed the photocurrent signal measured without optical bias and under front optical bias using two red and two blue optical signals modulated with multiple frequencies, which ensures the presence of 16 different combinations of the optical signals, and consequently the existence of 16 photocurrent levels. For this purpose, the driving currents of each LED emitter was adjusted to provide different levels of photo excitation.

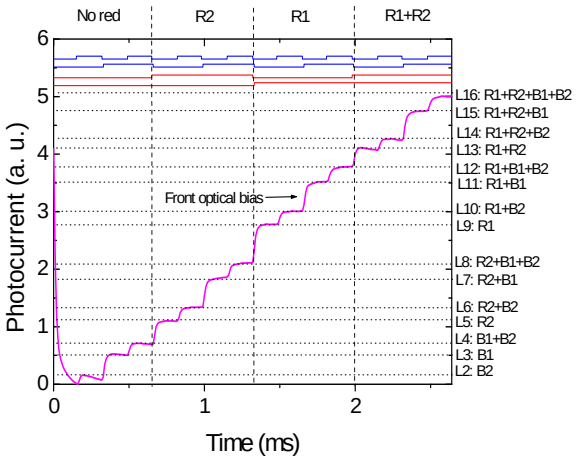

Fig. 10. Photocurrent signal measured under front optical bias using two red and two blue optical signals modulated with multiple frequencies (on the top it is displayed the waveform of the emitters modulation state).

Results show that when both red signals are off, the signals measured without and with front optical bias are quite similar, as the influence of the optical bias on this light wavelength is minimal. In the ranges labeled R2 and R1 only one red LED emitter is modulated together with the blue emitters of adjacent LEDs. The presence of the red light amplifies the photocurrent signal, and as the optical power delivered by each emitter has been deliberately adjusted at different levels, a clear separation of the photocurrent levels in both ranges is observed. Similar result is obtained when both red emitters (R1 and R2) are being simultaneously modulated, however, as the optical intensity is higher, the photocurrent levels of each optical excitation correspond also to higher levels. On the right side of the picture it is shown the label of the modulated emitters that correspond to each photocurrent levels.

The decoding of the transmitted optical signals through the evaluation of the threshold photocurrent demands the knowledge of the 16 possible levels, assigned to the 16 possible combinations. The absolute position of these levels is dependent on the optical intensity. However, the relative position among the levels is assumed to be constant, and this relation can be used to calibrate the assignment of the photocurrent levels to the optical signals. Despite, some adjacent photocurrent levels are very close and liable to wrong assignments, which results in mistakes on the content of the transmitted message. This apparent weakness of the decoding scheme is prone to generate bit error transmission and decreases the robustness of the transmission channel. Thus, bit error detection becomes a crucial tool to ensure a low bit error ratio. A smart strategy to enhance the robustness of transmission channel is using error detection codes, namely, parity or check bits. In this work, the parity bits (P1, P2, P3) assigned to the 4 transmission channels (Ch1, Ch2, Ch3, Ch4) are evaluated using a simple algorithm that sums up the bits transmitted by 3 of the channels:

$$\begin{aligned} P1 &= Ch1+Ch2+Ch4 \\ P2 &= Ch2+Ch3+Ch4 \\ P3 &= Ch1 + Ch3 + Ch4 \end{aligned} \quad (1)$$

In Fig. 11 it is displayed the parity check bits evaluated by Eq. (1) for the transmission of the bit sequences plotted in Fig. 10. Channels Ch1, Ch2 and Ch3 are assigned, respectively, to the emitters R1, R2, B1 and B2. The parity bits P1, P2 and P3 sequences are transmitted, respectively, by the R1, R2 and B1 emitters.

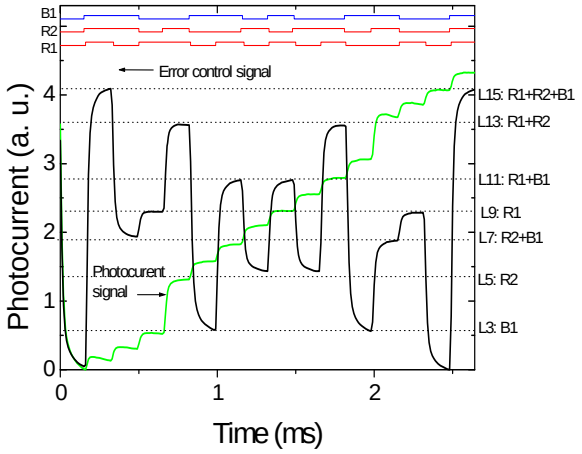

Fig. 11. Error control signal.

Results show that the error control signal can be used to help on the decode process when photocurrent level are very close. Levels L3 and L4, or levels L5 and L6, or even L7 and L8, that differ between themselves by a very narrow photocurrent magnitude may turn the decode process delicate, especially if intensity variations occur. However, as the error control signals associated to these levels are very different, the correct assignment can be done correctly. This methodology is suitable for the detection and correction of errors. Thus, data corruption can be easily corrected, without the need to discard the transmitted data from the specific error bit and re-transmit it again.

Results show that the error control signal can be used to help on the decode process when photocurrent level are very close. Levels L3 and L4, or levels L5 and L6, or even L7 and L8, that differ between themselves by a very narrow photocurrent magnitude may turn the decode process delicate, especially if intensity variations occur. However, as the error control signals associated to these levels are very different, the correct assignment can be done correctly. This methodology is suitable for the detection and correction of errors. Thus, data corruption can be easily corrected, without the need to discard the transmitted data from the specific error bit and re-transmit it again.

In Fig. 12 (a) it is displayed a random photocurrent signal measured under front optical bias using two red and two blue optical signals with different bit

sequences. As the bit sequences do not follow any specific pattern and correspond to independent messages, correct decoding, can be improved using the correspondent comparison with the error control signal obtained by parity check bits (Fig. 12(b).

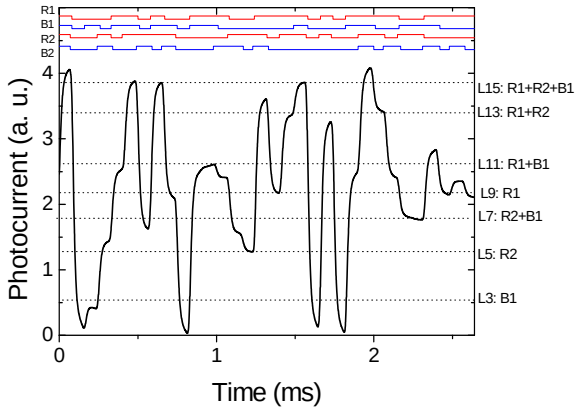

(a)

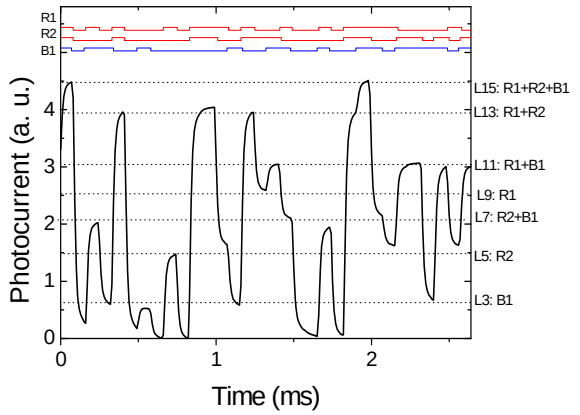

(b)

Fig. 12. a) Random photocurrent signal measured under front optical bias using two red and two blue optical signals with different bit sequences; b) Correspondent error control signal.

5. Conclusions

A spectral selective photodetector operating in the visible light spectrum was used to measure the output photocurrent supplied by red, green and blue emitters of RGB white LEDs in a visible light communication system. The device, designed specifically, to work as an active optical filter allowed the identification of the optical excitation of each of the emitters, and consequently the spatial position of the detector. Fourier analysis and device optical gains were used to perform the output signal decoding. A calibration curve was established to ensure signal decoding of random bits contained in the bits block of the message. Control bits strategy in the optical domain was implemented to reinforce the decoding procedure and improve system performance.

Acknowledgements

This work was sponsored by FCT – Fundação para a Ciência e a Tecnologia, within the Research Unit CTS – Center of Technology and systems, reference UID/EEA/00066/2019 and by project IPL/2019/Bid_VLC/ISEL and IPL/2020/GEO-LOC/ISEL.

References

[1]. E. Ozgur, E. Dinc, O. B. Akan, Communicate to illuminate: State-of-the-art and research challenges for visible light communications, *Physical Communication,* Vol. 17, 2015, pp. 72-85.

[2]. J. Armstrong, Y. Sekercioglu, A. Neild, Visible light positioning: a roadmap for international standardization, *IEEE Communications Magazine*, Vol. 51, Issue 12, 2013, pp. 68-73.

[3]. W. Zhang, S. Chowdhury, M. Kavehrad, Asynchronous indoor positioning system based on visible light communications, *Optical Engineering,* Vol. 53, Issue 4, 2014, pp. 045105-1 - 045105-9.

[4]. D. Karunatilaka, F. Zafar, V. Kalavally, R. Parthiban, LED based indoor visible light communications: State of the art, *IEEE Communications Surveys and Tutorials,* Vol. 17, Issue 3, 2015, pp. 1649 – 1678.

[5]. T. Komiyama, K. Kobayashi, K. Watanabe, T. Ohkubo, Y. Kurihara, Demonstration of Visible light Text data transmission system using LED lamp, in *Proceedings of the IEEE SICE Annual Conference*, 2011, pp. 1926-1928.

[6]. Z. Zhou, M. Kavehrad, P. Deng, Indoor positioning algorithm using light-emitting diode visible light communications, *Optical Engineering*, Vol. 51, Issue 8, 2012, p. 5009.

[7]. A. Jovicic, J. Li, T. Richardson, Visible light communication: opportunities, challenges and the path to market, *IEEE Communications Magazine*, Vol. 51, Issue 12, 2013, pp. 26-32.

[8]. Panta K., Armstrong J., Indoor localisation using white LEDs, *Electron. Lett.*, Vol. 48, Issue 4, 2012, pp. 228–230.

[9]. M. Vieira, M. Fernandes, A. Fantoni, P. Louro, R. Schwarz, A new CLSP sensor for Image recognition and color separation, *MRS Online Proceedings Library Archive*, Vol. 715, 2002.

[10]. P. Louro, V. Silva, M. A. Vieira, M. Vieira, Viability of the use of an a□SiC: H multilayer device in a domestic VLC application, *Physica Status Solidi (C) Current Topics In Solid State Physics*, Vol. 11, Issue 11–12, 2014, pp. 1703-1706.

[11]. M. A. Vieira, M. Vieira, V. Silva, P. Louro, M. Barata, Error control on spectral data of four□wave mixing based on a□SiC technology, *Physica Status Solidi (C)* Current Topics In Solid State Physics, Vol. 12, Issue 1–2, 2015, pp. 181-186.

[12]. P. Louro, M. Vieira, M. A. Vieira, Bidirectional data transfer in VLC links, *Proceedings SPIE 11302 Light-Emitting Devices, Materials, and Applications XXIV,* San Francisco, California, United States, 25 February 2020, pp. 1130214-1 - 1130214-11.

[13]. P. Louro, M. Vieira, J. Costa, M. A. Vieira, On-off keying transmitter design for navigation by visible light communication, *Proceedings SPIE 10538 Optical Interconnects XVIII,* San Francisco,

California, United States, 2018, pp. 1053809-1 – 1053809-9.
[14]. P. Louro, M. Vieira, M. A. Vieira, M Fernandes, J. Costa, Use of a-SiC: H photodiodes in optical communications applications, in Advances in Photodiodes (Gian-Franco Dalla Betta, Ed.), *IntechOpen*, Chapter 19, 2011, pp. 377-402.
[15]. P. Louro, *et al*., Optical demultiplexer based on an a□ SiC: H voltage controlled device, *Physica Status Solidi (C) Current Topics in Solid State Physics*, Vol. 7, Issue 3□4, 2010, pp. 1188-1191.
[16]. M. A. Vieira, M. Vieira, P. Louro, L. Mateus, P. Vieira, Indoor positioning system using a WDM device based on a-SiC:H technology, *Journal of Luminescence,* Vol. 191, 2017, 135-138.
[17]. P. Louro, M. Vieira, M. A. Vieira, Indoor Navigation Based on Visible Light Communication Using an a-SiC:H Photodetector, in *Proceedings of the 6th International Conference on Sensors Engineering and Electronics Instrumentation Advances (SEIA'2020)*, Porto, Portugal, 23-25 September 2020, pp. 167-173.
[18]. M. Vieira, M. A. Vieira, P. Louro, P. Vieira, Wayfinding in Large Environments Using Visible Light Communication, in *Proceedings of the 6th International Conference on Sensors Engineering and Electronics Instrumentation Advances (SEIA'2020),* Porto, Portugal, 23-25 September 2020, pp. 151-155.